Optics Communications 282 (2009) 4333–4338

Contents lists available at ScienceDirect

Optics Communications

journal homepage: www.elsevier.com/locate/optcom

Optimization for high precision Shack–Hartmann wavefront sensor

Chao Li [a,b], Mingliang Xia [a,b], Zhaonan Liu [a,b], Dayu Li [a], Li Xuan [a,*]

[a] State Key Lab of Applied Optics, Changchun Institute of Optics, Fine Mechanics and Physics, Chinese Academy of Sciences, Changchun, Jilin 130033, China
[b] Graduate School of the Chinese Academy of Sciences, Beijing 100039, China

ARTICLE INFO

Article history:
Received 17 March 2009
Received in revised form 24 July 2009
Accepted 27 July 2009

Keywords:
Shack–Hartmann wavefront sensor
Optical testing
Camera noise model

ABSTRACT

A comprehensive noise model about digital camera which is a main component of SHWFS is constructed, including the readout noise, the photon shot noise, the quantization noise and the response un-uniformity. Based on the noise model, the spot centroid errors caused by each kind of noise are analyzed, respectively. And then the synthetic error from all the noise is calculated. The result demonstrates that the limit of the spot centroid accuracy is 1% pixels. At last, the crossing error caused by the high order diffraction spots is analyzed. It is approximately proportional to the secondary spots number. So the structure of the microlens array must be optimized together with the digital camera when designing SHWFS.

1. Introduction

At the beginning of the 20th century, German astrophysicist Johannes Hartmann constructed a screen with a series of holes to test the optics of a large aperture telescope. The technology, Hartmann Screen test, remained unchanged for nearly 70 years. Until 1971, Roland Shack, who was involved in the study of measuring the telescope wavefront error in atmosphere, propounded to replace the holes in the Hartmann Screen with lenses in order to overcome the problem of extremely low illumination [1,2]. For the first time, the idea of measuring the dynamic wavefront error, at the same time an image of the satellite or star is taken by the ground-based telescope, seemed to be feasible. From then on, the Shack–Hartmann wavefront sensors (SHWFS) were widely used in the astronomical telescopes, and adaptive optics stepped in rapid development stage [3,4]. In 1994, Junzhong Liang firstly used SHWFS to measure the eye aberration and then realized the high-resolution retinal imaging through adaptive optics [5,6].

While SHWFS is a necessary instrument for adaptive optics, it is also widely used in other domain, such as optical calibration and alignment, metrology of thin transparent optics, beam diagnoses and so on [7–10]. And there are several important advantages to use SHWFS as the optical testing instrument. Unlike other beam diagnostic systems, SHWFS does not require moving parts. The incident radiation does not have to be coherent. The instrument provides a measure of both the irradiance and phase distributions of the incident light which is very useful for optical alignment. The SHWFS acquires all of the information from a single digital camera image, so short exposure times can be used to reduce the sensitivity to vibration and pulsed sources may be analyzed and aligned. The processing of the camera image is straightforward, simple, and may readily be performed on PC at high speed. Furthermore, except for the peak-to-valley (PV) wavefront deviation and the Root-Mean-Square (RMS) wavefront error, the point-spread-function (PSF), modulation transfer function (MTF) and Zernike wavefront decomposition can also be performed.

SHWFS can be configured for a variety of aperture sizes, wavelengths, sensitivities and dynamic ranges for different applications. There is great difference between the wavefront sensors used in astronomical adaptive optics and the ones for optical testing. In astronomical adaptive optics, it requires high light sensitivity to overcome low illuminant, and high working speed to realize the dynamic detection and real-time compensation for the wavefront aberration. And the low light signal-to-noise-ratio must be taken into consideration when designing and analyzing the performance of the wavefront sensor for adaptive optics. It was demonstrated a good choice to use a small quantity of pixels filling a subaperture of the wavefront sensor, such as 2×2 cells method [11]. This can improve the measurement precision and speed simultaneously. But in optical testing, the light source can be chosen or designed according to the requirement, especially the energy and wavelength. So it is feasible to improve the measurement precision further for the optical testing SHWFS by optimizing its configuration and the data processing method. In the paper, the factors affecting the measurement precision are analyzed, respectively and synthetically, in order to improve the performance of SHWFS.

* Corresponding author.
E-mail addresses: nk_lich@hotmail.com (C. Li), xuanli@ciomp.ac.cn (L. Xuan).

0030-4018/$ - see front matter © 2009 Elsevier B.V. All rights reserved.
doi:10.1016/j.optcom.2009.07.058

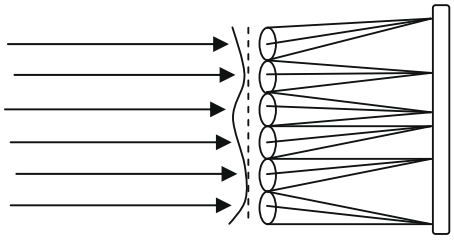

Fig. 1. The schematic configuration of the S–H wavefront sensor.

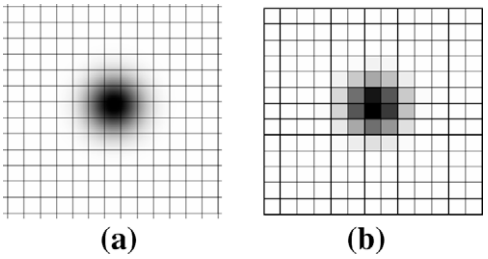

Fig. 3. The generation of the pixel signal. Each square denotes a pixel.

2. Theory and method

The Shack–Hartmann wavefront sensor usually comprises a lenslet array and a CCD or CMOS camera as is shown in Fig. 1. The lenslet array consists of a two-dimensional array of a few hundred lenslets, all with the same diameter and the same focal length. Each lenslet of the array is a sub-aperture of the wavefront sensor and several to several tens camera pixels fill in each sub-aperture. If the incident beam is ideal plane wavefront, the light spots will locate the center of each sub-apertures, otherwise the spots will be off centering corresponding to the local wavefront slope. And the wavefront can be decomposed from the local slopes through the least-square method. So the measurement precision of the wavefront is determined by the local slope precision, which is affected by the lenslet focal length and the center accuracy of the spot fundamentality. Although the longer focal length is helpful for increasing the local slope precision, the spot centroid accuracy will decay if the focal length is too long. So there would be a trade-off between the lenslet focal length and the center accuracy. Firstly the spot centroid calculation error will be analyzed.

$$\left.\frac{\partial W}{\partial x}\right|_i = \frac{x_i^t - x_i^0}{f}\left.\frac{\partial W}{\partial y}\right|_i = \frac{y_i^t - y_i^0}{f} \tag{1}$$

Ideally the centroid position of a light spot with profile $I(x,y)$ should be calculated as

$$Xc = \frac{\int I(x,y)x\ dx}{\int I(x,y)\ dxdy} \quad Yc = \frac{\int I(x,y)y\ dx}{\int I(x,y)\ dxdy} \tag{2}$$

For an ideal photodetector array of finite size and quantity, the detected centroid position of light spot would be

$$Xc = \sum_{i,j}^{L,M} P_{ij}X_i \Big/ \sum_{i,j}^{L,M} P_{ij} Yc = \sum_{i,j}^{L,M} P_{ij}Y_j \Big/ \sum_{i,j}^{L,M} P_{ij} \tag{3}$$

where $P_{ij} = \delta_{ij} \cdot \alpha \int_{\Delta Sij} I(x,y)\ \ dxdy$ and ΔS_{ij} is the area of the (i,j) pixel, δ_{ij} denotes the photon response non-uniformity (PRNU) of the camera, α denotes the photon-to-signal ratio which consists of the quantum efficiency and the A/D conversion factor, L and M are the number of pixels in X- and Y-direction, respectively within a sub-aperture.

Furthermore, take the photodetection noise into consider, formal (3) would be

$$Xc = \sum_{i,j}^{L,M}(P_{ij} + \sigma_{ij})X_i \Big/ \sum_{i,j}^{L,M}(P_{ij} + \sigma_{ij})$$
$$Yc = \sum_{i,j}^{L,M}(P_{ij} + \sigma_{ij})Y_j \Big/ \sum_{i,j}^{L,M}(P_{ij} + \sigma_{ij}) \tag{4}$$

The discrete sampling from formula (2) to formula (3) will induce sampling error, quantization error and PRNU error for the centroid calculation. And the photodetection noise in formula (4) contains photon shot noise, readout noise and dark current noise.

Although many authors have analyzed the centroid calculation error [11–13], they paid more attention on the low-light-level wavefront measurement and did not take other factors into consideration, such as PRNU and quantization error. In order to minimize the numerical simulation error, we analyzed all the error factors based on the camera signal noise model shown in diagram Fig. 2 [14]. And the first kind and zero order Bessel function is used to descript the distribution of the spot intensity instead of Gauss function. But the environment background noise is not considered because it can be eliminated by improving the light source and the experiment environment.

Fig. 3 illustrates the numerical simulation method. A two-dimension intensity distribution with the ideal center (x_0, y_0) is simulated from the Bessel function. It is divided by the simulated pixels as is shown in Fig. 3a and the intensity is integrated in each pixel area to generate the pixel signal shown in Fig. 3b. Then centroid (x_c, y_c) of the spot is calculated by formula (3). So the centroid calculation error can be estimated by the difference between (x_c, y_c) and (x_0, y_0). The unit used in the simulation is unit "1", that is to say the spot position, spot size, pixel position and pixel size are all with the same unit "1". But the centroid error is expressed with unit pixel. For example, pixel size 10, FWHM of the spot 15 and centroid error 1% pixel means that the spot is mainly sampled by two pixels and the absolute centroid error is 0.1.

3. Simulation result

The sampling error is analyzed firstly in order to determine the proper sample ratio for analyzing the other factor errors. In our calculation, the FWHM of the spot is set 15, the sampling sub-window is −90 to +90 and the generated ideal spot center moves from (−35, 0) to (35, 0). By changing the pixel size, the sampling error is calculated (shown as Fig. 4). The error curve behaves like the cosine function, which is mainly caused by the sparse discrete sampling and the Bessel type of the light spot distribution. Further

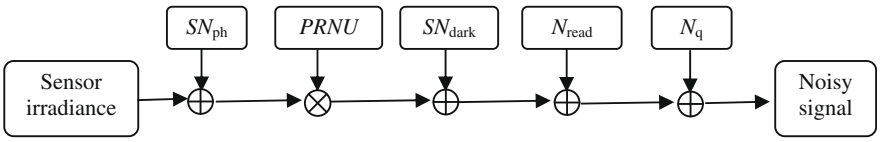

Fig. 2. The noise model for the signal capture in digital camera.

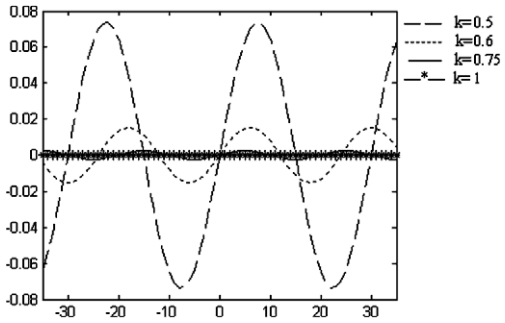

Fig. 4. Sampling error of the centroiding in *X*-direction. *k* is the ratio between the spot FWHM and the pixel size.

analysis illustrates that, when the spot is sampled symmetrical by the surrounding pixels the error is zero and vice versa. It can be seen that, as the sample ratio *k* (the ratio of the spot FWHM and the pixel size) increases, the sampling error decreases sharply. When the ratio is 0.75, the maximum error is about 0.3% pixel. When the ratio is 1 and 1.25, the maximum error is only 3.1×10^{-5} pixel and 1.3×10^{-5} pixel, respectively which can be neglected. In order to test the sampling error for $k = 1.25$ furtherly, we calculate the sampling error for 500 random points (center position of the simulated spot) locating in the square area $(-30, -30)$ to (30, 30) as is shown in Fig. 5a. The sampling errors are expressed in the form of histogram in Fig. 5b. So in the following, we choose $k = 1.25$ (pixel size 12) to calculate the other noise errors. And the spot is mainly sampled by 4×4–5×5 pixels for $k = 1.25$.

Because the other noise is closely relative with the characters of camera, a simulated camera is constructed with the key parameters listed in Table 1. All the parameters are not critical for the scientific camera commonly used now. And in the following calculation, the maximum pixel signal is set 15,000e, a little smaller than the full well depth.

Due to the quantum character of light, the capture of photons is a Poisson process that arises from random fluctuations in sampling when discrete quanta are measured. So the photon shot noise is the nature of light. The standard deviation of the photon shot noise is equal to the square root of the average number of photons, i.e. $\sigma_{ph} = \sqrt{N}$, where *N* is the average number of photons shooting in one pixel. Then the signal-to-noise-ratio for shot noise is $SNR_{ph} = \sqrt{N}$. As the number of photons increases, the SNR will be enhanced. In this simulation step, the maximum signal after integration is set 30,000 photons (corresponding 15,000e) and the signals in other pixels are zoomed with the same scale. Then the shot noise is generated according to each signal value and added into the signal. The centroid error was calculated for 500 points randomly falling in the area $(-30, -30)$–(30, 30) and the result is shown in Fig. 6a.

Table 1
The key parameters of the simulated camera.

Pixel size	12
PRNU	1–2%
Full well capacity	16,000e
Quantum efficiency	50%
Readout noise	16e (type)
Dark current	50e/pixel/s
Dynamic range	1000
Digital depth (adjustable)	8bit, 10bit, 12bit
Readout noise	16e

Table 2
The statistical results of the centroid errors. Unit (pixels).

No.	Max (%)	Min (%)	Std (%)
(a)	−0.71	0.69	0.22
(b)	−1.06	1.25	0.38
(c)	−0.56	0.53	0.20
(d)	−10.30	8.90	3.73
(e)	−0.58	0.62	0.19
(f)	−0.72	0.63	0.21
(g)	−0.16	0.21	0.05
(h)	−0.06	0.05	0.02
(i)	−2.40	2.20	0.72
(j)	−1.95	2.43	0.65
(k)	−2.03	2.37	0.66
(l)	−1.43	1.34	0.41
(m)	−1.09	1.06	0.39
(n)	−1.06	1.08	0.39

The photon response non-uniformity is caused by variations in pixel geometry and substrate material of the photoreceptor. Since PRNU is caused by the physical properties of a sensor, it is nearly impossible to eliminate and usually considered a normal characteristic of the sensor array. Typically the non-uniformity is only 1–2%. In the section, all the other factors are neglected and each signal is multiplied by a random parameter which normally distributes in the range 0.98–1.0 or 0.99–1.0 for PRNU 2% and 1%. The result for 500 times calculation is shown in Fig. 6b and c. When the PRNU is 2%, the maximum possible error reaches 1% pixels. And the maximum error reduces to 0.5% pixels when PRNU is 1%.

Readout noise is generally defined as the combination of the remaining circuitry noise between the photoreceptor and the

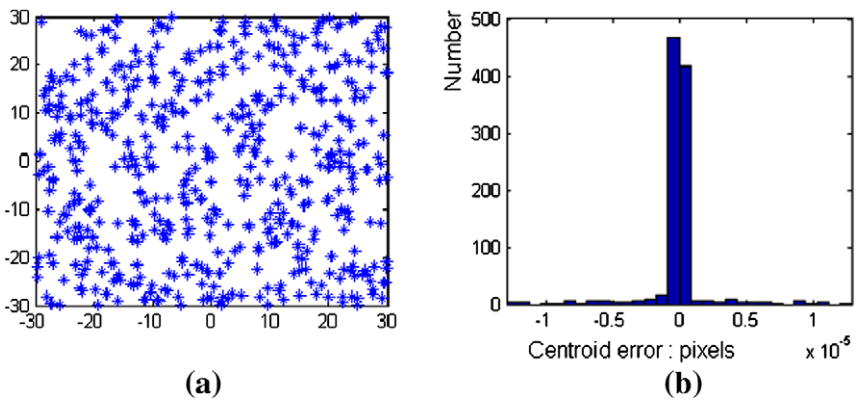

Fig. 5. The distribution of the light spot center and the sampling error. The histogram contains both the centroid errors in *X*-direction and *Y*-direction. The maximum value, minimum value and the standard deviation is 1.29×10^{-5}, -1.31×10^{-5}, 2.1×10^{-6} pixels, respectively.

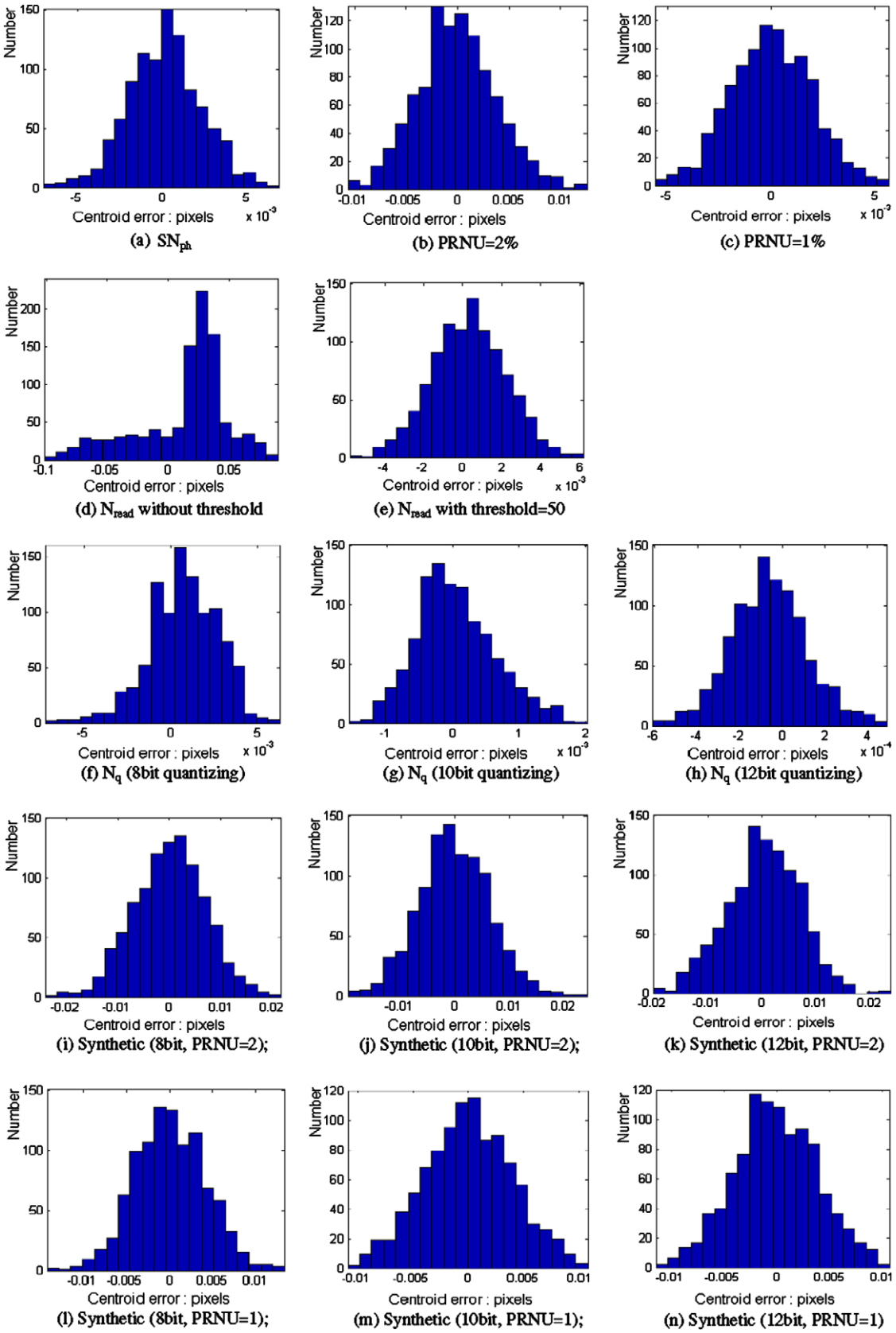

Fig. 6. The centroid error for different conditions. From (a) to (h), every one is only about one factor. From (i) to (n), all the factors are analyzed synthetically and every one corresponded to a combination of quantization level and PRNU. The statistical results of centroid error are listed in Table 2.

ADC circuitry including pixel reset noise, thermal noise, and other minor contributors like conductor shot noise. Dark current noise has the similar statistical character as readout noise and usually it is very small. For example, if the exposure times is 0.02 s, the

dark current noise is only 1e typically which can be neglected. So it is added into the readout noise in the section. Fig. 7 shows the signals after the readout noise added. The impact of readout noise is so severely that the error reaches 10% pixels as is shown in Fig. 6d. The main reason is that the useful signal distributes in only a small part of the whole window while the readout noise is full of the window. So the threshold method is adoptable [11]. The signal value which is smaller than the threshold is not taken into the centroid calculation. When the threshold is set 50, about three times of the noise, the error is only 0.6% pixels as is shown in Fig. 6e. Some other thresholds are also calculated, and the improvement is similar as threshold 50e. But the improvement will decay obviously, if the threshold is smaller than two times of the noise or larger than five times.

The conversion of non-trivial analogue signal to the digital domain results in rounding errors during the quantization process. For signal variations much larger than the quantization step, the noise added to the signal is approximate

$$\sigma_q^2 = \frac{q^2}{12} \tag{5}$$

where q is the quantizing step.

In this section, we do not take the method of adding random noise into the signal directly, but process the raw pixel signal after integration like the real digital camera. Firstly all the pixel signal is zoomed with the same ratio to make the maximum signal is 15,000e, near the full capacity. Then the signal is divided by 62.5. At last rounding operation is taken on the signal. This is just the A/D conversion process for 8bit quantizing level. Ten bit and 12bit level quantizations are also calculated and the results are shown in Fig. 6f–h. As the quantizing level increases, i.e. the quantizing step decreases, the centroid error induced by only quantization noise diminishes.

From the results we can see that, as single error factor the PRNU (2%) is prominent, photon shot noise is secondly. And the centroid errors caused by other kind of noise individually are all smaller than 1% pixels. Although the error caused by readout noise can reach 10% pixels, it is only 0.6% pixels with a proper threshold.

At last the centroid calculation accuracy is estimated synthetically, that is all the kinds of noise are taken into calculation simultaneously. Because there are three quantization levels (8bit, 10bit and 12bit) and two levels about PRNU (1% and 2%), each combination of the two factors is calculated. What's more, the threshold method is still used to reduce the impact of readout noise. The results are shown as Fig. 6i–n. If the PRNU is 2%, the centroid error is above 2% pixels no matter what level the quantization is. When the PRNU is 1%, the centroid errors for 10bit and 12bit quantization reduce to 1% pixels. Further calculation demonstrates that, when the sampling ratio is 1 or larger than 1.25 (from 1.5 to 4 is calculated), the synthetic centroid error is almost the same as $k = 1.25$. And if the maximum photon number falling in one pixel is set more than 1,00,000, which means that the SNR_{ph} enhances, the maximum centroid error could reduce to 0.9% pixels.

4. Further consideration

The error of wavefront local slope is also associated with the focal length of the lenslet. For the same spot centroid accuracy, the longer the focal length, the smaller the slope error will be. But with the focal length increasing, the size of the main diffraction spot and the crossing of the high order diffraction spots will also increase, which will induce crossing error for the spot centroid calculation [15]. Fig. 8 shows the diffraction pattern of a 5×5 microlens array with focal length 6 mm and sub-aperture diameter 0.15 mm. When calculating the crossing error, a group of random wavefront local slope (25 different values) was set to the lenslet array. So, the light spot will depart from the center of each microlens as shown in Fig. 8b. The centroid error was calculated only for the central 9 microlens and the root-mean-square-value of the 9 error values was calculated as the mean error.

The crossing error is calculated for simulated microlens with diameter 0.1 and 0.15 mm as is shown in Fig. 9. It should be emphasized that,when calculating the spot centroid the sub-window method is used to reduce the impact of high order diffraction spots [11]. The secondary spots number N between two main spots can be written as:

$N = \frac{D^2}{\lambda f^{-2}}$ where D is the diameter of the microlens, f is the focal length and λ is the wavelength which is set 0.6 μm in the calculation. As the secondary spot number decreases, i.e. the focal length lengthens, the crossing error increases. So there is a tradeoff between the focal length of the lenslet and the spot centroid calcula-

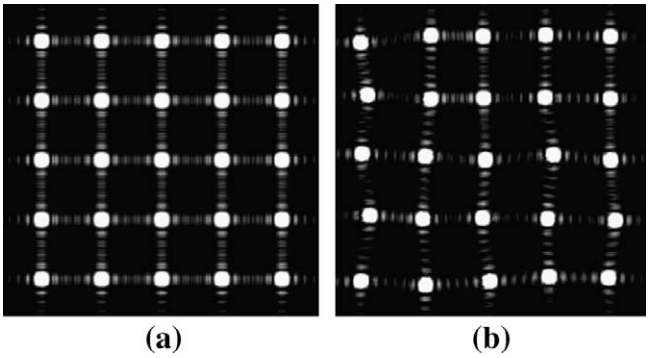

Fig. 8. The diffraction pattern of microlens array with focal length 6 mm and diameter 0.15 mm. (a) is the ideal pattern and (b) is the pattern with random wavefront local slope. The maximum departure of the spots for pattern (b) is 30 μm, 1/5 of the microlens diameter.

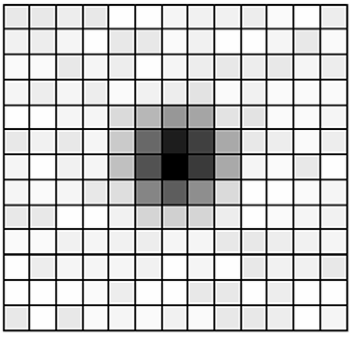

Fig. 7. The signals with readout noise added.

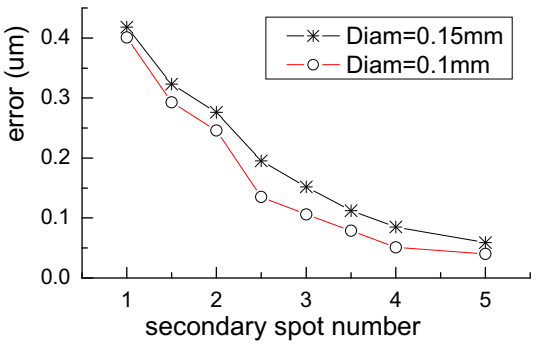

Fig. 9. The crossing error caused by high order diffraction spots.

tion precision. Besides, the dynamic range of SHWFS will reduce when the focal length is longer. All of these must be kept in mind when constructing a SHWFS for high precision measurement.

5. Conclusion

As a main component of SHWFS, the digital camera is also the main error origin for wavefront measurement. So a comprehensive noise model about the digital camera is constructed, including the main noise origins such as photon shot noise, PRNU, readout noise and so on. The impact of each kind of noise is analyzed, respectively. The results demonstrated that the discrete sampling error could not be neglected unless the sampling ratio is larger than 1. The response uniformity is a key factor for the spot centroid calculation and the uniformity of 1% will be sufficient for realizing 1% pixels centroid accuracy. Although the error caused by 8bit quantization noise is smaller than 1% pixels, using higher quantization level would be a good choice and 10bit digital depth camera is very common now. Besides, it is necessary to use threshold method to diminish the impact of readout noise and by the method the centroid accuracy can be improved by a factor of 10.

Because the wavefront measurement precision is determined by the accuracy of wavefront local slope, which is proportional to the focal length of lenslet, increasing the focal length is helpful for improving the precision. However, the crossing error will increase and the dynamic range will decrease as the focal length lengthens. So the structure of lenslet array must be optimized when designing SHWFS.

Acknowledgments

This work is supported by National Natural Science Foundation (Nos. 60578035, 50473040 and 60736042) and Science Foundation of Jilin Province (Nos. 20050520, 20050321, and 20050322).

References

[1] Ben C. Platt, Roland Shack, J. Refract. Surg. 17 (2001) 573.
[2] R.V. Shack, B.C. Platt, J. Opt. Soc. Am. 61 (1971) 656.
[3] A.J.W. Hardy, Proc. SPIE 1542 (1991) 2.
[4] R.Q. Fugate et al., J. Opt. Soc. Am. A 11 (1994) 310.
[5] J. Liang, B. Grimm, S. Goelz, J.F. Bille, J. Opt. Soc. Am. A 11 (1994) 1949.
[6] J. Liang, R. Williams, T. Miller, J. Opt. Soc. Am. A 14 (1997) 2884.
[7] S. Goelz, J.J. Persoff, G.D. Bittner, J. Liang, Proc. SPIE 1542 (1991) 502.
[8] D.R. Neal, W.J. Alford, J.K. Gruetzner, Proc. SPIE 2870 (1996) 72.
[9] Craig R. Forest, Claude R. Canizares, Daniel R. Neal, Opt. Eng. 43 (2003) 742.
[10] Grupo de Óptica Aplicada, Departamento de Física, Universidad Nacional de Colombia, Ciudad Universitaria, Opt. Commun. 263 (2006) 17.
[11] S. Thomas, Proc. SPIE 5490 (2004) 1238.
[12] Genrui Cao, Xin Yu, Opt. Eng. 3 (1994) 2331.
[13] D.L. Asha, C.J. Solomona, G. Loos, Opt. Commun. 156 (1998) 10.
[14] K. Irie, A.E. McKinnon, K. Unsworth, I.M. Woodhead, Meas. Sci. Technol. (2008) 19.
[15] Yang Dai, Faquan Li, Xuewu Cheng, Opt. Laser Tech. 39 (2007) 1374.